On interfacial properties of tetrahydrofuran: Atomistic and coarse-grained models from molecular dynamics simulation

J. M. Garrido,[1] J. Algaba,[2] J. M. Míguez,[3,4] B. Mendiboure,[3] A. I. Moreno-Ventas Bravo,[5] M. M. Piñeiro,[4] and F. J. Blas[2,a)]

[1]*Departamento de Ingeniería Química, Universidad de Concepción, POB 160-C Concepción, Chile*
[2]*Laboratorio de Simulación Molecular y Química Computacional, CIQSO-Centro de Investigación en Química Sostenible and Departamento de Física Aplicada, Universidad de Huelva, 21007 Huelva, Spain*
[3]*Laboratoire des Fluides Complexes et Leurs Reservoirs, Université de Pau et des Pays de l'Adour, CNRS, TOTAL–UMR 5150, Avenue de l'Université, B.P. 1155, Pau F-64013, France*
[4]*Departamento de Física Aplicada, Universidade de Vigo, E36310 Vigo, Spain*
[5]*Laboratorio de Simulación Molecular y Química Computacional, CIQSO-Centro de Investigación en Química Sostenible and Departamento de Geología, Universidad de Huelva, 21007 Huelva, Spain*

(Received 16 October 2015; accepted 22 March 2016; published online 11 April 2016)

We have determined the interfacial properties of tetrahydrofuran (THF) from direct simulation of the vapor-liquid interface. The molecules are modeled using six different molecular models, three of them based on the united-atom approach and the other three based on a coarse-grained (CG) approach. In the first case, THF is modeled using the transferable parameters potential functions approach proposed by Chandrasekhar and Jorgensen [J. Chem. Phys. **77**, 5073 (1982)] and a new parametrization of the TraPPE force fields for cyclic alkanes and ethers [S. J. Keasler *et al.*, J. Phys. Chem. B **115**, 11234 (2012)]. In both cases, dispersive and coulombic intermolecular interactions are explicitly taken into account. In the second case, THF is modeled as a single sphere, a diatomic molecule, and a ring formed from three Mie monomers according to the SAFT-γ Mie top-down approach [V. Papaioannou *et al.*, J. Chem. Phys. **140**, 054107 (2014)]. Simulations were performed in the molecular dynamics canonical ensemble and the vapor-liquid surface tension is evaluated from the normal and tangential components of the pressure tensor along the simulation box. In addition to the surface tension, we have also obtained density profiles, coexistence densities, critical temperature, density, and pressure, and interfacial thickness as functions of temperature, paying special attention to the comparison between the estimations obtained from different models and literature experimental data. The simulation results obtained from the three CG models as described by the SAFT-γ Mie approach are able to predict accurately the vapor-liquid phase envelope of THF, in excellent agreement with estimations obtained from TraPPE model and experimental data in the whole range of coexistence. However, Chandrasekhar and Jorgensen model presents significant deviations from experimental results. We also compare the predictions for surface tension as obtained from simulation results for all the models with experimental data. The three CG models predict reasonably well (but only qualitatively) the surface tension of THF, as a function of temperature, from the triple point to the critical temperature. On the other hand, only the TraPPE united-atoms models are able to predict accurately the experimental surface tension of the system in the whole temperature range. © *2016 AIP Publishing LLC.* [http://dx.doi.org/10.1063/1.4945385]

I. INTRODUCTION

Tetrahydrofuran, c-$(CH_2)_4O$ or simply THF, is a cyclic ether widely used as solvent in many industrial processes. One of its various applications is the use as thermodynamic hydrate promoter.[1,2] This molecule is able to form structure II (sII) hydrates[1] when mixed in stoichiometric ratio with water (17 H_2O molecules per THF molecule), at 277.15 K and atmospheric pressure. From an applied point of view, its effect on systems exhibiting hydrate phases is very important, because it produces a pronounced shift on the hydrates coexistence curves when used as an additive. This ability has been widely exploited to produce hydrates in appropriated temperature and pressure ranges depending on the application envisaged. As an example, several authors[3–5] used THF for applications as the reduction of the equilibrium pressure of H_2 clathrate hydrates, considering its application in H_2 storage cells,[6,7] and of carbon dioxide (CO_2) hydrates for environmental concerns related with greenhouse gas emission control and effects on global climate change.[8–11]

During the last decades, remarkable progresses have been made on the development and application of the so-called molecular modeling techniques for the prediction of thermodynamic properties (i.e., phase equilibrium and interfacial properties) of an important number of complex mixtures of industrial interest. Examples of these methods

a)Electronic mail: felipe@uhu.es

are theoretical approaches based on a microscopic vision of the system, such as perturbation theories, Density Gradient Theory (DGT), or Density Functional Theory (DFT), and computer simulation methodologies,[12–16] including Monte Carlo (MC) and Molecular Dynamics (MD). This wide range of techniques is being applied and used nowadays for the determination of equilibrium and non-equilibrium properties of hydrates, including phase equilibrium, and particularly the dissociation line of the hydrate phases (see, e.g., Míguez *et al.*[17] and references therein), and other properties, such as kinetic and structural properties.[2]

The success of these methods in predicting accurately the behaviour of complex mixtures depends critically on how precisely the chemical structure and intermolecular and intramolecular potential energies between the components of the system are known. This includes not only traditional systems that exhibit fluid-fluid phase equilibrium, but also systems that show hydrate phases, including carbon dioxide, methane, and THF hydrates. Different approaches to describe intermolecular potential of molecules as carbon dioxide, methane, and even water, have been extensively studied during last decades. However, the case of THF is different. Although this molecule is widely used as solvent in many processes, very limited work has been devoted to the determination of its thermodynamic properties, and phase equilibria in the case of mixtures of industrial interest.

For this reason, THF molecular models are scarce in literature. The first one was proposed in the 1980s by Jorgensen and collaborators in the context of the Transferable Parameters Potential Functions (TIPS), a series of force fields suitable for use in liquid simulations for water, alcohols, and ethers. In the seminal work of TIPS,[18–20] the interaction sites for this molecule are located on oxygen, hydroxyl hydrogens, and the carbons in the alkyl groups, each site combining Coulombic and Lennard-Jones parameters chosen to yield reasonable structural and energetic results for both gas-dimers and pure liquids of water, alcohol (methanol and ethanol), and ethers. The model for THF in this framework was proposed by Chandrasekhar and Jorgensen.[21,22] In particular, they considered Monte Carlo simulations of liquid THF and solutions in water, methanol, and also THF with and without pseudo-rotation of the cyclic ether. As for other TIPS models, the intermolecular potentials consist of Lennard-Jones and Coulomb terms, in the same way as those reported previously for ethers.[23] Several years later, Jorgensen and co-workers proposed the well-known Optimized Potential for Liquid Simulations—or OPLS—force fields,[24,25] which can be regarded as an evolved version of the former TIPS approach. Unfortunately, the authors did not determine THF vapor-liquid coexistence, neither using TIPS or OPLS approaches.

More recently, Helfrich and Hentschke[26] and Girard and Müller-Plathe[27] examined several THF force fields and simulated different bulk and structural properties, although none of them considered the simulation of the vapor-liquid coexistence. Finally, Keasler *et al.*[28] developed a new version of the TraPPE-UA force field (Transferable Parameters for Phase Equilibria-United Atoms) specifically for five- and six-membered cyclic alkanes and ethers, including THF. In particular, they took into account that partial charges are molecule specific and thus they were parametrized using liquid-phase dielectric constants. This THF model is able to provide accurate saturated liquid densities and vapor pressures, critical temperatures and densities, and other important thermodynamic properties. Unfortunately, none of the works cited determined THF interfacial properties.

On the other hand, there has been an increasing effort during the last years in developing new coarse-grained (CG) intermolecular potential functions for the fluid state based on alternative top-down techniques. The usual bottom-up methodology, which is based on quantum-mechanical or atomic-level description of the interactions between real molecules, integrates out some (unwanted) degrees of freedom of the real system through different techniques and uses iterative simulation procedures to refine the parameters of the model. Examples of this methodology are the well known all-atom and united-atom force fields existing in the literature since the early 1980s. Following an opposite philosophy, the top-down methods are based on the use of an accurate equation of state to link macroscopic properties of the fluid state and force field parameters.[29] One of the most promising alternatives is based on the group-contribution formulation of the statistical associating fluid theory (SAFT-γ).[30–32] The specific version of this approach for molecules formed from heteronuclear chemical groups that interact through the Mie intermolecular potential,[33] referred to as SAFT-γ Mie,[34] based on the latest enhanced version of the SAFT-VR Mie,[35] can be used to estimate the corresponding force field. This information can then be used in direct simulations to obtain a great variety of thermodynamic, structural, interfacial, and dynamic properties. This top-down approach has neither been used so far to describe THF thermodynamic or interfacial properties. Another interesting point is that the ability of CG molecular models to describe complex real interfacial behavior has been pointed out recently for the case of multicomponent mixtures,[36] leading to a pertinent discussion concerning the comparison of their quantitative performance if compared with their counterpart atomistic molecular models.

Although the accurate description of bulk thermodynamic properties and phase equilibrium is essential to any sound molecular model, not every standard property determined routinely from computer simulation exhibits the same sensitivity to the details of theoretical molecular models. However, fluid-fluid interfacial properties, and particularly surface tension, are one of the most sensitive properties to subtle differences in molecular details. These properties play a key role in many different fields, including nucleation or dynamics of phase transitions, and their knowledge is essential in a great number of practical and industrial applications. This has attracted the attention from simulators of the liquid community over the last years, allowing nowadays the accurate determination of these properties from computer simulation using different methodologies. Among all of them, surface tension is obviously the most important and challenging property to be determined and predicted in the context of inhomogeneous systems.[12,14,15]

This work is the first of a series of papers in which models of THF and mixtures with other substances are developed and tested to predict accurately the phase equilibrium

and interfacial properties of these systems using computer simulation. The long-term goal of this work is to use the proposed molecular models to predict the phase equilibrium of THF hydrates and hydrates of mixtures of THF with methane and/or carbon dioxide. The particular objectives of this work are two. Firstly, to use some models existing in the literature for predicting the vapor-liquid interfacial properties of THF; and secondly, to propose new CG molecular models for THF, based on the SAFT-γ Mie, able to describe the vapor-liquid phase equilibrium and interfacial properties of THF. In all cases, results obtained from MD simulation are compared with recommended experimental data[37] to critically assess the models ability. To our knowledge, this is the first time that the vapor-liquid interfacial properties, and particularly the surface tension, of THF are determined from computer simulations.

The rest of the paper is organized as follows. In Sec. II we summarize the molecular models considered, as well as the simulation details. Results and discussion are presented in Section III. Finally, in Section IV we present the main conclusions.

II. MOLECULAR MODELS AND SIMULATION DETAILS

A. SAFT-γ coarse grained Mie force field

As follows from the generic SAFT approach,[38,39] the Helmholtz energy function of a fluid can be described on an additive basis as a contribution of several molecular effects

$$a = \left(a^{MONO} + a^{CHAIN} + a^{IDEAL}\right)\rho\frac{N_{av}}{\beta}. \quad (1)$$

In the particular case of the SAFT-γ Mie model—which has been selected for performing Coarse-Grained molecular simulation—the mathematical structure of each contribution has been discussed in detail by Lafitte *et al.*[35] Briefly in Eq. (1), $a = A/(Nk_BT)$ and A is the total Helmholtz energy, N is the total number of molecules, N_{av} is the Avogadro constant, T is the temperature, k_B is the Boltzmann constant, $\beta = 1/(k_BT)$, and ρ is the molar density of the fluid. a^{MONO} represents a monomer (unbound) contribution for a chain composed of m_s tangential segments, a^{CHAIN} accounts for the formation of chain molecules, and a^{IDEAL} is the ideal gas contribution.

In the framework of CG force fields, the pure fluids will be modeled as freely jointed tangential non associating spheres characterized by five parameters: the molecular chain length (or number of segments) m_s, the repulsion and attraction parameters of the intermolecular potential λ_r and λ_a, the energy scale or potential well depth ε, and the length scale, roughly equivalent to a segment diameter σ, which can be found from three alternative routes. The first or traditional way is to force the EoS to fit the available fluid phase equilibrium data (experimental measurements or molecular simulation data), (i.e., vapor pressure and liquid density data), and second derivative properties.[40] A second option is using the corresponding states principle,[41,42] in terms of conformational parameters of the Mie potential. In the latter case, as it was recently demonstrated, once m_s and λ_a are fixed, the remaining parameters can be calculated using the acentric factor (which defines the λ_r value), critical temperature (which defines the ε value), and the liquid density evaluated at 0.7 of the critical temperature (which defines the σ value). Finally, following the general methodology proposed by Segura *et al.*,[43,44] the molecular parameters of pure fluids can be calculated by forcing the EoS to exactly reproduce the experimental vapor pressure, the local slope of the vapor pressure curve, and the density and compressibility of the liquid phase at one single reference temperature in terms of the theory of displacements.[45,46]

TABLE I. SAFT-γ Mie CG force field parameters for THF.

m_s	ε/k_B (K)	σ (Å)	λ_r	λ_a	Reference
1[a]	668.797	5.401	47.07	6.00	41
2[b]	348.920	3.840	14.85	6.00	41
3[c]	261.632	3.350	13.63	6.00	This work
3[d]	277.080	3.359	13.63	6.00	This work

[a]Monomer configuration.
[b]Dimer configuration.
[c]Ring configuration.
[d]Refined parameters for the Ring configuration.

In this work we modeled THF as a single- and double-segment pearl-necklace model, without any additional electrostatic interactions, estimated from the corresponding states principle (or critical data) proposed by Mejía *et al.*[41] This methodology has shown great flexibility to characterize vapor-liquid interfacial properties of pure fluids[47] and complex mixtures of dilute surfactant solutions[48] and natural gases and condensates.[47,49–51] Table I summarizes the SAFT parameters for THF as used in molecular simulations in this work. Nevertheless, the methodology proposed by Mejía *et al.*[41] cannot be used directly in a rigid configuration, because energy contribution in Eq. (1) due to the formation of m_s-membered ring from a theoretical point of view is different.[52–54] Firstly, the approximation in the Helmholtz energy contribution of ring structures (i.e., $a^{RING} \approx -m_s \ln g^{Mie}(\sigma)$) suggested by Lafitte *et al.*[55] has been used to obtain initial values of force field parameters. It has been noted that the protocol generalized by Segura *et al.*[43,44] allows a great compromise between the properties of the pure fluid and the SAFT-γ Mie model. This means, of course, that the theoretical description will not provide a perfect match between theory and molecular simulation. Indeed, following the *recipe* provided in Refs. 40 and 55–57 force field parameters of the rigid model (σ,ε) have been rescaled to match the simulation results with the theoretical prediction and recommended experimental data from DECHEMA.[37] Table I summarizes also a set of SAFT-γ parameters for the THF three-segment ring configuration. On one hand, model 3c in Table I corresponds to a set of model parameters recommended for use in theoretical predictions for fluid properties of THF. On the other hand, force fields of model 3d (refined parameters) are recommended for use in molecular simulations. The reader is referred to Ref. 55 for further details.

B. United-atom force field models

As we have mentioned, THF has been also modeled following the united-atom approach. We use three different

models to describe this cyclic ether. In all cases, the force fields use the Lennard-Jones and Coulomb potentials to describe the non-bonded interactions,

$$U(r_{ij}) = 4\epsilon_{ij}\left[\left(\frac{\sigma_{ij}}{r_{ij}}\right)^{12} - \left(\frac{\sigma_{ij}}{r_{ij}}\right)^{6}\right] + \frac{q_i q_j}{4\pi\epsilon_0 r_{ij}}, \qquad (2)$$

where r_{ij} is the distance between interacting sites i and j, σ_{ij} and ϵ_{ij} are the diameter and well depth associated to the LJ intermolecular potential, q_i and q_j are the partial charges on interaction sites i and j, and ϵ_0 the permittivity of vacuum. All the LJ parameters for unlike interactions are obtained always using the Lorentz-Berthelot combining rules.

In all the united-atoms models used in this work, THF molecule is described with three different types of united-atom chemical groups. The ether group or oxygen atom, O, the α-methyl (α-CH_2) united atoms bonded directly to the oxygen atom, and the β-methyl (β-CH_2) united atoms bonded to the α-methyl chemical group. In addition to that, partial charges are placed on the interaction sites of the oxygen atom and the α-CH_2 and β-CH_2 chemical groups. Molecular parameters for the LJ diameter and well depth of different chemical units, as well as values of partial charges are given in Table II.

We first consider the rigid version of the model proposed by Chandrasekhar and Jorgensen,[21,22] in which THF can be viewed as a planar and rigid cyclic ether. In this case, since the molecule is rigid, nor bending neither torsional intramolecular potentials are needed. Molecular parameters due to the non-bonded interactions between THF molecules are collected in Table II. Note that, apart from the negative partial charge located at the ether group to account for its electronegativity, the α-CH_2 chemical groups have positive partial charges allowing the model to mimic the molecular electric dipole moment. However, the β-CH_2 groups do not have any partial charge associated. This is probably one of the most important differences between this model and the TraPPE-UA model. As we will see in the following, this and other differences in the molecular parameters produce important differences in the thermodynamic and interfacial properties estimations.

We also consider the original TraPPE model of Keasler *et al.*[28] In this model, as usual in TraPPE force fields, the bond lengths between different chemical groups are fixed. Monomeric units separated by two bonds interact through a harmonic bending potential with the usual form, with bending force constants taken from the TraPPE-UA force field for n-alkanes and ethers.[28] Interactions between beads separated by three bonds are described through a torsional intramolecular potential energy represented by a cosine series.[28] For further details on the TraPPE-UA force field we recommend the original paper of Keasler *et al.*[28]

Finally, following a similar approach than the case of the Chandrasekhar and Jorgensen model, we consider an approximated, planar, and rigid TraPPE model, in which non-bonded LJ intermolecular parameters and partial charges located at the different chemical groups are identical to those of the original TraPPE model. In addition to that, bending and torsional degrees of freedom are frozen, i.e., we consider that the equilibrium bond angles are fixed and the molecule has no torsional degrees of freedom. As an additional approximation, THF is considered in this case not only rigid but also planar.

TABLE II. TraPPE-UA and Jorgensen force field parameter for non-bonded interactions of THF.

Atom	ε/k_B (K)	σ[Å]	q[e]
THF (TraPPE-UA)			
O	190	2.20	−0.410
$CH_2(\alpha)$	56.3	3.88	0.160
$CH_2(\beta)$	56.3	3.88	0.045
THF (Jorgensen)			
O	85.47	3.00	−0.5
$CH_2(\alpha)$	59.39	3.80	0.25
$CH_2(\beta)$	59.39	3.905	0.0

C. Simulation details

All MD simulations are carried out in conditions at which the vapor-liquid interface is present, following the standard methodology[16,58] for all models studied. In particular, simulations are performed in the *NVT* canonical ensemble using GROMACS (version 4.6.1)[59] at a fixed temperature T, in a parallelepipedic simulation cell of constant volume $V = L_x \times L_y \times L_z$, where L_x, L_y, and L_z are the dimensions of the simulation box. We use periodic boundary conditions in all three directions. A homogeneous liquid system is first equilibrated in a rectangular simulation box of dimensions $L_x = L_y = 14\sigma$ and $L_z = 32\sigma$. We consider $N = 12\,500$, 6250, 2800 for systems formed from 1, 2, and 3 monomers in the case of CG models (see Table I) and 2430 molecules for UA simulations. After equilibration of this bulk-liquid system, the box is expanded to three times its original size along the z direction leaving the liquid phase slab at the center. The final overall dimensions of the vapor-liquid-vapor configuration box are therefore $L_x = L_y = 14\sigma$, and $L_z = 92\sigma$ for each system. In order to reduce the truncation and system size effects involved in the phase equilibrium and interfacial properties calculations, the cut-off radius (r_c) has been taken equal to a large value of 7σ. It has been shown by several authors[60–62] that a cut-off above six diameters provides a reliable description for the interfacial properties. However, it was shown by Dinpajooh *et al.*,[63] it is thus natural to consider larger cut off values when the objective is obtain a reliable predictions of critical properties. Long-range interactions are determined using three-dimensional Ewald technique with a convergence parameter of 0.1 Å^{-1} and a maximum value for the reciprocal lattice equal to 31 is used.

We have used a Verlet leapfrog[64] algorithm with a time step of 0.002 ps for the case of CG models, Jorgensen-UA (rigid model), and the simplified TraPPE-UA model (rigid model). It is important to note in this case that a time step of 0.001 ps has been necessary to sample correctly the torsional potential in the case of rigorous TraPPE-UA model (flexible model). A Nosé-Hoover thermostat[65] with large time constant equal to 1.0 ps has been used. After the system reaches equilibrium, the properties of the coexisting vapor and liquid phases can be obtained as appropriate averages during 10 ns (including an equilibration period of 5 ns). In order to estimate

errors on the variables computed, the sub-blocks average method has been applied.[66] In that approach, the production period is divided into n independent blocks. The statistical error is then deduced from the standard deviation of the average $\bar{\sigma}/\sqrt{M}$, where $\bar{\sigma}$ is the variance of the block averages and M has been fixed in this work to $M = 10$.

The equilibrium vapor pressure, P_v, and interfacial tension, γ, are obtained from the diagonal components of the pressure tensor. The vapor pressure corresponds to the normal component, $P_v = P_{zz}$, of the pressure tensor, while the interfacial tension is obtained using the mechanical route[13,67–69] as

$$\gamma = \frac{L_z}{2}\left[P_{zz}(z) - \frac{P_{xx}(z) + P_{yy}(z)}{2}\right]. \quad (3)$$

In Eq. (3), the additional factor 1/2 comes from having two interfaces in the system, and L_z is the size of the simulation box in the z direction, defined along the longitudinal dimension across the interface. The critical pressure, P_c, temperature, T_c, and density, ρ_c have been obtained from the vapor-liquid equilibrium results, presented in Tables III and IV, using the scaling laws[12,70] given by

$$\rho_L - \rho_V = A(T - T_c)^{\beta} \quad (4)$$

and the corresponding law of rectilinear diameters

$$\frac{\rho_L + \rho_V}{2} = \rho_c + B(T - T_c) \quad (5)$$

β is the corresponding critical exponent, with a universal value of $\beta = 0.325$,[13] and A, B, T_c, and ρ_c are four unknown constants obtained fitting to the simulation results. ρ_L and ρ_V are the liquid and vapor coexistence densities at the corresponding temperature T. Alternatively, an independent way to calculate T_c is to apply the scaling laws for the case of interfacial calculations.[71] Following this route, γ is related to T_c by the following expression:

$$\gamma = \gamma_0(1 - T/T_c)^{\mu}, \quad (6)$$

where γ_0 is the so-called "zero-temperature" surface tension and μ is the corresponding critical exponent. Here, we fix μ to the universal value $\mu = 1.258$ as obtained from renormalization-group theory.[13] Once again, the unknown constants, γ_0 and T_c are found by fitting the interfacial tension data with temperature. Finally, the critical pressure is estimated from an extrapolation of the Clausius-Clapeyron relation to the critical temperature obtained from Eq. (4) or

TABLE III. Vapor pressure P, liquid density ρ_L, vapor density ρ_V, 10-90 interfacial thickness d, and surface tension γ at different temperatures for CG force fields of THF formed from tangentially bonded segments (m_s). The errors are estimated as explained in the text.

m_s	T/K	P/MPa	ρ_L/(kg/m^3)	ρ_V/(kg/m^3)	d/nm	γ/(mN/m)
1[a]	300	0.0017(2)	868.8(3)	0.347(8)	0.768(5)	27.5(9)
	325	0.007(1)	829.7(2)	1.91(1)	0.887(5)	25.5(7)
	350	0.156(2)	813(2)	4.12(2)	1.305(3)	21.9(7)
	375	0.29(1)	775(2)	7.74(4)	1.153(2)	17.7(7)
	400	0.56(2)	749(2)	13.6(5)	1.848(3)	14.5(5)
	425	0.88(3)	724.4(3)	21.89(5)	1.64(3)	11.0(9)
	450	1.451(4)	673(3)	34.8(6)	2.17(2)	8.1(7)
	475	2.18(4)	629(3)	52.7(6)	2.52(2)	6.9(4)
	500	3.118(7)	579(3)	80.9(1)	3.356(9)	3.5(6)
	520	4.028(9)	531(3)	110.3(1)	3.96(3)	2.6(9)
2[b]	300	0.002(2)	881.3(2)	0.656(9)	0.747(2)	28.78(7)
	325	0.043(2)	853(2)	1.791(1)	0.823(6)	26.94(7)
	350	0.132(2)	822(2)	3.16(3)	0.959(4)	22.27(7)
	375	0.24(2)	792.6(2)	7.44(4)	1.121(4)	20.03(8)
	400	0.487(2)	758.5(2)	12.34(2)	1.57(3)	15.13(9)
	425	0.87(3)	722.6(2)	20.3(5)	1.675(3)	13.15(5)
	450	1.40(2)	686(3)	33.2(4)	1.903(2)	8.94(7)
	475	2.07(5)	640(3)	50.7(6)	2.221(1)	7.05(7)
	500	3.111(8)	588(3)	79.9(1)	2.78(9)	3.93(9)
	520	4.081(1)	536.4(3)	105.7(1)	3.87(1)	1.95(9)
3[c]	300	0.006(9)	883.1(3)	0.444(8)	0.685(4)	28.91(7)
	325	0.026(2)	854.8(2)	1.614(1)	0.789(4)	25.7(1)
	350	0.14(2)	823.8(2)	3.01(2)	0.917(3)	23.39(4)
	375	0.25(2)	792(2)	6.62(4)	1.07(5)	19.22(7)
	400	0.531(2)	758(2)	12.12(2)	1.317(7)	15.59(5)
	425	0.89(4)	719.1(3)	19.9(5)	1.532(2)	12.59(9)
	450	1.405(3)	681(3)	31.2(4)	1.67(3)	8.39(4)
	475	2.153(7)	634.8(3)	52.7(6)	2.381(7)	5.49(6)
	500	3.177(7)	579(3)	83.6(1)	1.72(3)	3.35(7)
	520	4.22(8)	514(4)	121.4(1)	4.36(5)	1.37(9)

[a]Monomer configuration.
[b]Dimer configuration.
[c]Refined parameters for the ring configuration (see Table I).

TABLE IV. Vapor pressure P, liquid density ρ_L, vapor density ρ_V, 10-90 interfacial thickness d, and surface tension γ at different temperatures by the different UA force fields for THF. The errors are estimated as explained in the text.

UA-model	T/K	P/MPa	ρ_L/(kg/m^3)	ρ_V/(kg/m^3)	d/nm	γ/(mN/m)
Jorgensen	200	−0.002(6)	978(6)	0.0(0)	0.4050(8)	46.0(5)
	250	−0.002(9)	930(3)	0.0(0)	0.537(3)	38.4(2)
	300	0.02(1)	881(3)	0.0(0)	0.693(1)	30.7(1)
	350	0.11(1)	830(3)	3.07(13)	0.883(4)	24.1(1)
	400	0.42(4)	775(3)	9(1)	1.122(1)	18.0(1)
	450	1.14(6)	713(3)	25.8(8)	1.53(2)	11.5(1)
	500	2.45(8)	633(3)	58.5(9)	2.01(1)	6.4(1)
	525	3.3(2)	582(8)	87.7(3)	2.76(1)	3.9(1)
	550	4.41(8)	495(6)	135.7(9)	3.82(1)	2.2(2)
Rigid TraPPE	200	−0.002(8)	964(3)	0.0(0)	0.431(8)	41.3(1)
	250	−0.001(9)	913(3)	0.113(2)	0.58(2)	32.9(1)
	300	0.045(1)	861(3)	1.22(1)	0.754(5)	26.5(1)
	325	0.086(2)	834(3)	2.35(2)	0.857(7)	22.9(1)
	350	0.209(2)	805.4(3)	5.2(3)	1.14(1)	19.9(1)
	375	0.37(3)	775.4(2)	9.1(4)	1.208(7)	16.5(2)
	400	0.67(5)	742.3(2)	16.2(6)	1.37(5)	13(1)
	425	1.085(6)	708(3)	26.4(6)	1.514(3)	11(1)
	450	1.67(9)	669.4(2)	41.1(8)	2.01(3)	7.5(2)
	475	2.4(1)	622(3)	60.5(8)	2.166(4)	4.6(1)
	500	3.5(1)	560(3)	98(1)	3.20(2)	3.3(1)
TraPPE	200	−0.35(3)	974.4(3)	0.0(0)	0.404(3)	40.5(1)
	250	−0.34(4)	923.51(3)	0.08(6)	0.565(5)	34.3(4)
	300	−0.31(7)	872.3(4)	1.01(4)	0.743(4)	27.4(1)
	350	−0.167(7)	817(5)	4.97(5)	0.952(4)	20.5(1)
	400	0.26(1)	756(1)	14.74(9)	1.346(2)	14.3(1)
	450	1.28(5)	681.3(3)	38.32(1)	1.734(2)	8.8(1)
	500	2.918(4)	584(8)	83.04(3)	3.31(2)	3.7(1)

TABLE V. Experimental and predicted critical properties of THF with different force fields models[a]

Source	Models	ρ_c (kg/m^3)	T_c^a/K	T_c^b/K	P_c/MPa
Experimental[37]	...	320	541	...	5.2
MD *NVT*	CG-monomer	307(14)	545(8)	552(7)	5.9(2)
MD *NVT*	CG-dimer	307(12)	546(5)	549(4)	5.4(4)
MD *NVT*	CG-RING	307(16)	540(4)	542(5)	5.3(1)
MD *NVT*	Jorgensen	318(16)	572(7)	578(6)	5.1(5)
MD *NVT*	Rigid TraPPE	308(15)	540(6)	537(6)	5.9(3)
MD *NVT*	TraPPE	312(11)	543(6)	552(5)	5.5(6)
GEMC[28]	TraPPE	328(4)	544(2)	...	5.5(6)

[a]Critical densities (ρ_c) of THF with different force fields models as obtained from the analysis of the coexistence densities using Eqs. (4) and (5); critical temperatures (T_c^a) of THF with different force fields models as obtained from the analysis of the coexistence densities using Eqs. (4) and (5); critical temperatures (T_c^b) of THF with different force fields models as obtained from the analysis of the computed tension data using Eq. (6) and fixing the critical point to $\mu = 1.258$; and critical pressure (P_c) of THF with different force fields models as obtained from the analysis of Eq. (7).

Eq. (6)

$$\ln P = C_1 + \frac{C_2}{T}, \tag{7}$$

where C_1 and C_2 are correlation parameters. Results obtained in this work from the analysis of the simulation data using Eqs. (4)–(7) are presented in Table V.

III. RESULTS AND DISCUSSION

In this section we present the main results from the simulations of tetrahydrofuran (THF) using three different coarse grained models and three different UA models. We focus on the interfacial properties, such as density profiles, interfacial thickness, and surface tension. We also examine the temperature dependence of these properties, and compare our results for the different models with literature experimental data.[37] In particular, we compare the results corresponding to predictions from the different coarse grained models and the three UA models considered in this work.

We follow the same analysis and methodology as in our previous works,[72–75] and consider different temperatures for all the models analyzed. In order to characterize the bulk phase and interfacial behaviour, density profiles are calculated by dividing the system in 250 slabs along the z direction. The molecular density profiles, $\rho_i(z)$, are obtained by assigning the position of each united atom center, z_i, to the corresponding slab and constructing the molecular density from mass balance considerations. The bulk vapor and liquid densities in each system are obtained by averaging $\rho_i(z)$ over appropriate regions sufficiently removed from the interfacial region. In addition to that, the final bulk vapor density value, at each temperature and chain length, is obtained after averaging the density profiles on both sides of the liquid film. Another interesting property that can be obtained from the calculation of density profiles is the interfacial width along the liquid-vapor equilibrium. Implicitly this property is defined by fitting the curves from the original mean field van der Waals theory,[12,13] described by

$$\rho(z) = \frac{\rho_L + \rho_V}{2} - \frac{\rho_L - \rho_V}{2} \tanh\left[\frac{\alpha(z - z_0)}{d}\right], \tag{8}$$

where the constant $\alpha = 2\tanh^{-1}(0.8)$ is chosen so that d is the 10-90 interfacial thickness and z_0 the position of the Gibbs dividing surface. As mentioned, coexistence densities have been calculated previously, therefore d and z_0 are treated as adjustable parameters in Eq. (8). As for the calculation of the bulk vapor density, our reported values of d correspond to the average of the values for both interfaces in the system. Values determined this way are always found to be coincident to within statistical uncertainty; indicating that the inhomogeneous systems are properly equilibrated at all temperatures. The statistical uncertainty of these values is estimated from the standard deviation of the mean values. For the six THF models studied here, Tables III and IV summarize the numerical values of the MD simulations and the corresponding statistical deviations.

We show in Fig. 1 the density profiles $\rho(z)$ for the coarse grained model of THF with two Mie spherical segments (dimer model) and for the rigid UA TraPPE model. For

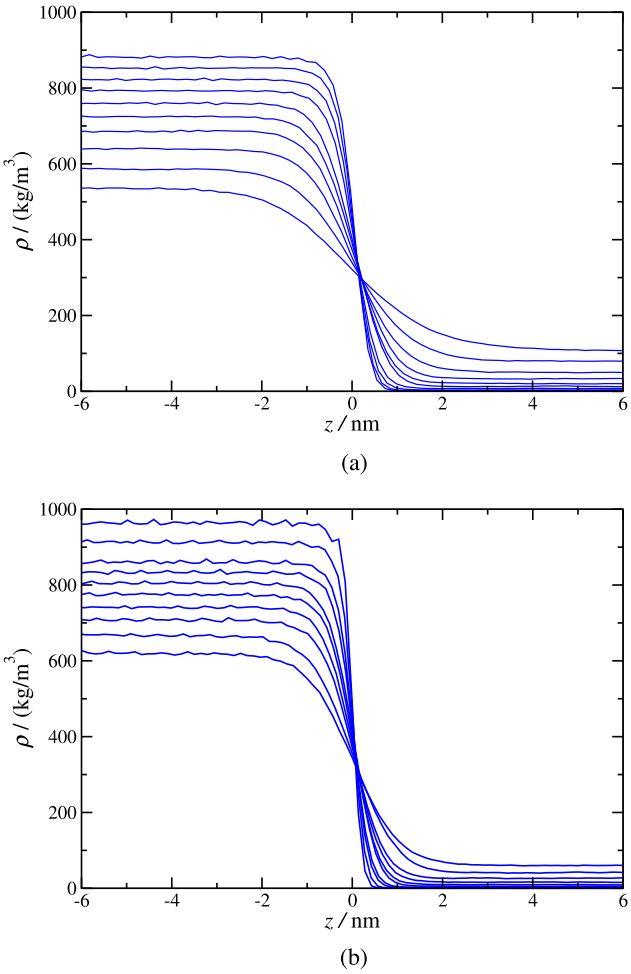

FIG. 1. Simulated equilibrium density profiles across the vapor-liquid interface of THF as obtained from MD *NVT* simulations using the coarse grained dimer (a) and the rigid TraPPE model (b). From bottom to top (in the liquid region): (a) 300, 325, 350, 375, 400, 425, 450, 475, 500, and 525 K, (b) 200, 250, 300, 325, 350, 375, 400, 425, 450, and 475 K.

the sake of clarity, we only present one half of the profiles corresponding to one of the interfaces. Also for convenience, all density profiles have been shifted to place z_0 at the origin. As can be seen, density profiles for both approaches provide similar values of the liquid and vapor densities at the same temperatures. Liquid density decreases and vapor density increases as the temperature is increased as expected. In addition to that, the absolute value of the slope of the density profiles in the interfacial region decreases as the temperature is increased. This is an expected behavior as the critical temperature of the system is approached. This is also in agreement with the divergence, as it is shown later, of the interfacial thickness as $T \to T_c$. For the other CG and UA models, we have checked that results are equivalent.

We have also estimated the location of the critical point resulting from our direct MD simulations. The critical coordinates (temperature, T_c, density, ρ_c, and pressure, P_c) are obtained following the procedure explained in Section II. In Table V we report the values of the critical temperatures, densities, and pressures as obtained from this procedure. In addition to that, we have also included the literature THF critical coordinates.

The vapor-liquid phase envelopes of the different CG and UA models for THF are depicted in Fig. 2. We have also included the experimental data[37] corresponding to the coexistence curve of THF. We first analyze the phase behavior of THF as obtained from MD *NVT* simulations of the three CG models. As can be seen, the predictions obtained from the three models, i.e., monomer, dimer, and ring CG, are very similar and in excellent agreement with literature experimental data in the whole range of temperatures from near the triple-point to the critical temperature.[37] We have also represented in the same figure the phase behavior predicted from simulations of

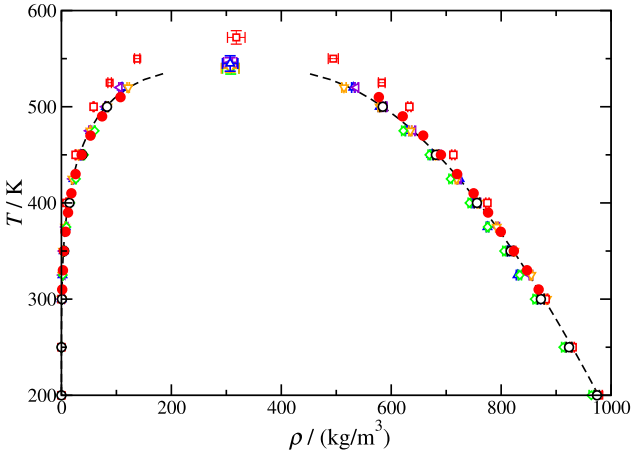

FIG. 2. Vapor-liquid coexistence densities for THF. The symbols correspond to the coexistence densities obtained from the MD *NVT* simulations for the CG monomer (empty blue triangles up), the CG dimer (empty left violet triangles), and the CG ring (empty orange triangles down) models, the UA of Jorgensen (empty red squares), the flexible UA TraPPE model (empty black circles), and the rigid UA approximated TraPPE model (empty green diamonds). Results for the flexible UA TraPPE model using GEMC[28] (filled red circles) are shown also in the figure. The dashed curve corresponds to the experimental coexistence densities taken from DECHEMA.[37] Symbols at the highest temperature for each coexistence curve represent the critical points estimated from Eqs. (4) and (5), for more details see Table V.

the UA models. As can be seen, the UA of Jorgensen is only able to predict quantitatively the vapor-liquid phase behavior at low temperatures, below 350 K, approximately. At higher temperatures, the model overestimates the coexistence liquid density and underestimates the vapor density. Contrarily, the other two UA models studied are able to provide a quantitative description of the phase envelope of THF. Agreement between experimental data and estimations from the TraPPE model is better in the case of the original version since the rigid or approximated TraPPE model proposed in this work slightly underestimates the saturated liquid density of THF.

Surprisingly, the approximated TraPPE model proposed here is able to predict reasonably well the experimental vapor-liquid phase envelope of THF. This is important since flexible models, that include bending and torsional intramolecular potentials, need MD time steps considerably shorter that rigid models. This is a restriction coming from the necessity to solve correctly the Newton's equations of motion associated to the internal degrees of freedom of these molecules. In this particular case, MD *NVT* simulations for the (fully) flexible TraPPE model need twice more CPU time than those corresponding to the rigid TraPPE model to simulate the same real time evolution of the system. This is an important issue that should be taken into account when dealing when simulating explicit interfaces, as they need remarkably longer CPU times if compared to homogeneous phases.

We have also calculated the vapor pressure of the THF models. In this particular case, since we are dealing with a planar interface and simulations are performed using MD *NVT* simulations, the vapor pressure is equal to the normal (perpendicular to the interface) component of the pressure tensor P_N. These results are shown in Tables III and IV. It is somewhat striking to check that these simulations may produce negative values of vapor pressure at low temperatures, as seen for UA models in Table IV. The reason for this is that, as already pointed out by Vega and de Miguel,[76] the direct coexistence is not the most accurate method to determine vapor liquid coexistence conditions, specially when dealing with low temperatures corresponding to very low vapor pressures, where the sampling of this technique produces larger deviations. Instead, if the vapor liquid coexistence is to be evaluated accurately, Gibbs ensemble would be a more convenient choice, as it allows remarkable efficiency if conveniently implemented, as discussed recently for instance by Cortés-Morales *et al.*[77]

Recalling that the main objective of this work is the determination of interfacial properties, we will focus first on interfacial thickness of THF (cf. Table I). We have included the results obtained from simulations for the three CG models, as well as for UA models. Fig. 3 shows its temperature trend for the different models tested. As shown, d increases with temperature, which simply reflects the fact that the interfacial region gets wider, as can be also observed in Fig. 2. At low temperatures the density profiles exhibit a sharp interface which corresponds to a low value of the interfacial thickness. As the temperature is increased towards the critical value the interfacial region becomes wider, and hence, the value of the interfacial thickness increases and diverges as $T \to T_c$. Note that all models exhibit the same qualitative behavior.

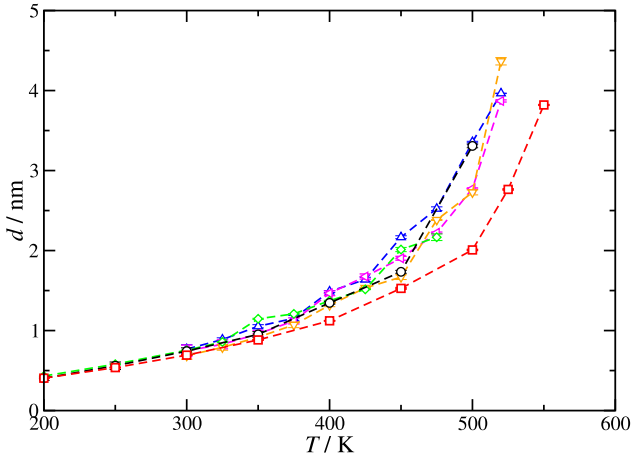

FIG. 3. Interfacial thickness d as a function of temperature for THF. The meaning of the symbols is the same as in Fig. 2. The dashed curves are included as a guide to the eye.

The only exception is the case of the Jorgensen UA. This may be explained in terms of the predictions obtained from this model in Fig. 2. As can be seen, the UA model of Jorgensen overestimates liquid density and underestimates vapor density, predicting consequently a wider vapor-liquid phase separation at higher temperatures ($T \sim 400$ K). A higher width in densities in $T\rho$ phase diagrams indicates a higher slope in the density profile at the interfacial region, and consequently, a higher surface tension, as shown also in Fig. 4. As we have mentioned previously in this section, the differences between the predictions of the Jorgensen models with the other models considered here are probably due to a wrong description of the distribution of the point charges in the α- and β-methyl chemical groups.

We finally consider the behavior of the vapor-liquid surface tension of THF. In particular, we compare the results obtained in this work for the coarse grained models and the UA of Jorgensen, Keasler *et al.*, and the rigid version of the formed model. As we have mentioned previously in this section and in Section I, interfacial properties, and particularly surface tension, are extremely sensitive to molecular model

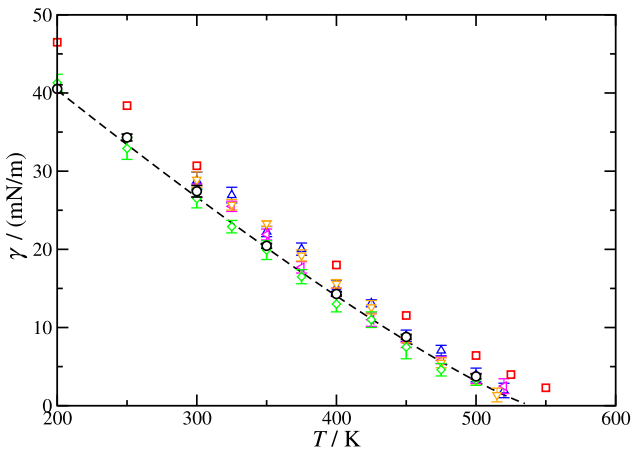

FIG. 4. Surface tension as a function of temperature for THF. The meaning of the symbols and dashed curves is the same as in Fig. 2.

details of the system. The temperature dependence of the surface tension for all models is shown in Fig. 4. As can be seen, the values of the interfacial tension predicted by the coarse grained and the Jorgensen model are above the experimental values. This is especially true for the case of the UA model of Jorgensen, that fails in predicting the surface tension for the whole temperature range considered. Deviation between simulation results and experimental data, in the case of coarse grained models, is lower, especially at high temperatures. Finally, both TraPPE models (rigid and flexible) are able to provide a quantitative description of the experimental vapor-liquid surface tension of THF in the whole range of temperatures, from the triple-point up to the critical temperature. The original TraPPE model seems to be slightly more accurate than the approximated rigid TraPPE model near the critical temperature. However, MD *NVT* simulations for the former model are faster (up to twice those corresponding to the flexible model), and this should also be taken into account when simulating the vapor-liquid interface of this kind of molecules.

IV. CONCLUSION

We have determined the interfacial properties of the vapor-liquid interface of THF considering two different approaches for modeling the system. In the first approach, three different coarse grained force fields based on the SAFT-γ Mie molecular equation of state are used. Under this approach, THF is modeled as a single sphere, as a diatomic molecule, and as a ring formed from three Mie monomeric units. In the second approach, we use three different united atoms models, including the TIPS model proposed by Chandrasekhar and Jorgensen, the TraPPE model by Keasler and collaborators, and an approximated rigid version of this latter model proposed in this work.

We use MD *NVT* simulations of the inhomogeneous system containing two vapor-liquid interfaces. The surface tension is evaluated from the calculation of the normal and tangential components of the pressure tensor from the virial route. We have examined the density profiles, interfacial thickness, and surface tension in terms of temperature. In addition to that, we have calculated the coexistence phase envelope and vapor pressure, including the location of the critical point from an analysis of the density profiles and the surface tension. All properties have been determined for the six molecular models studied. Predictions obtained from MD simulation are compared with experimental data taken from the literature for all properties except for the case of interfacial thickness.

The vapor-liquid phase envelope of THF is predicted remarkably well by the three CG models proposed. In particular, agreement between experimental literature data and predictions from the CG dimer model are comparable with the best united atoms models used in this work. Both TraPPE models, the approximated rigid version and the full flexible model, are able to provide an excellent accuracy in the whole coexistence range. The original TraPPE model proposed by Keasler *et al.* predicts more accurately

the saturated liquid density at low temperatures than the approximated version of the model. This is expected since the model parameters have been obtained to ensure the correct vapor-liquid coexistence behavior. Unfortunately, the united-atoms model by Jorgensen is unable to predict correctly the phase envelope at intermediate to high temperatures, close to the critical region. In particular, the model overestimates the liquid density and underestimates the vapor density. The CG models are also able to predict very accurately the vapor pressure, as a function of temperature, and particularly the CG dimer model. The original TraPPE model reproduces the experimental vapor pressure of the system at all temperatures very accurately. The approximated rigid version of the model provides a reasonably good agreement with experimental data at low and intermediate temperatures, but unfortunately overestimates the vapor pressure at high temperatures. The Jorgensen model underestimates the vapor pressure in the whole range of temperatures at which the seem exhibits vapor-liquid coexistence.

Finally, we have used the six models to predict the vapor-liquid surface tension of THF. The CG models are only able to predict qualitatively the behavior of the surface tension, as a function of temperature. In particular, these models overestimate the experimental data taken from the literature at intermediate and low temperatures. Nevertheless, the agreement between both results is remarkable, bearing in mind that molecular models are usually fitted only to experimental saturated liquid density and vapor pressure,[37] without using any information on interfacial properties. The only united atoms model able to predict accurately THF vapor-liquid surface tension is the TraPPE model, including the original version and the approximated rigid model proposed in this work. The Jorgensen model is unable to predict quantitatively the surface tension, overestimating their values at all temperatures. This is in agreement with the poor description of the vapor-liquid phase envelope, probably due to a wrong election of the molecular parameters of the ether and methyl functional groups, including the distribution of the partial charges assigned. On the contrary, both TraPPE models provide a quantitative and excellent description of the surface tension along the complete temperature range. Although the original TraPPE model seems to predict the surface tension better than the approximated rigid model proposed in this work, the planar and rigid model is faster for simulating since internal degrees of freedom are frozen (neither bending nor torsional intramolecular interactions need to be evaluated). This is an important and clear advantage, especially when interfacial properties need to be calculated and in the case of mixtures containing other chemical compounds. We are currently investigating the advantage of this model for simulating vapor-liquid and liquid-liquid interfaces of binary mixtures containing THF.

ACKNOWLEDGMENTS

We thank Dr. Andres Mejía (Universidad de Concepción, Chile) for stimulating discussions. This work was supported by Ministerio de Economía and Competitividad (MINECO, Spain) through Grant Nos. FIS2013-46920-C2-1-P and FIS2015-68910-P, both cofinanced with EU FEDER funds. We also acknowledge CESGA (www.cesga.es) in Santiago de Compostela, Spain, and MCIA (Mésocentre de Calcul Intensif Aquitain) of the Universités de Bordeaux and Pau et Pay de l'Adour, France, for providing access to computing facilities. J.M.G. acknowledges the doctoral scholarship from Conicyt (Chile) and from Red Doctoral REDOC.CTA, MINEDUC Project No. UCO1202 at U. de Concepción. J.M.M. acknowledges Xunta de Galicia (Spain) for the Postdoctoral Grant. J.A.F. acknowledges Contrato Predoctoral de Investigación from XIX Plan Propio de Investigación de la Universidad de Huelva. Further financial support from Junta de Andalucía, Universidad de Huelva, and Carnot Institure (ISIFoR, France) are also acknowledged.

[1]R. Larsen, C. A. Knight, and E. D. Sloan, Fluid Phase Equilib. **150**, 353 (1998).
[2]E. D. Sloan and C. Koh, *Clathrate Hydrates of Natural Gases*, 3rd ed. (CRC Press, New York, 2008).
[3]L. J. Florusse, C. J. Peters, J. Schoonman, K. C. Hester, C. A. Koh, S. F. Dec, K. N. Marsh, and E. D. Sloan, Science **306**, 469 (2004).
[4]H. Lee, J. W. Lee, D. Y. Kim, J. Park, Y. T. Seo, H. Zeng, I. L. Moudrakovski, C. I. Ratcliffe, and J. A. Ripmeester, Nature **434**, 743 (2005).
[5]T. A. Strobel, C. A. Koh, and E. D. Sloan, Fluid Phase Equilib. **261**, 382 (2007).
[6]V. V. Struzhkin, B. Militzer, W. L. Mao, H.-K. Mao, and R. J. Hemley, Chem. Rev. **107**, 4133 (2007).
[7]H. P. Veluswamy, R. Kumar, and P. Linga, Appl. Energy **122**, 112 (2014).
[8]S. P. Kang and H. Lee, Environ. Sci. Technol. **34**, 4397 (2000).
[9]M. Ricaurte, C. Dicharry, D. Broseta, X. Renaud, and J.-P. Torré, Ind. Eng. Chem. Res. **52**, 899 (2013).
[10]P. Babu, R. Kumar, and P. Linga, Energy **50**, 364–373 (2013).
[11]P. J. Herslund, K. Thomsen, J. Abildskov, N. von Solms, A. A. Galfre, P. Brantuas, M. Kwaterski, and J.-M. Herri, Int. J. Greenhouse Gas Control **17**, 397 (2013).
[12]J. S. Rowlinson and F. L. Swinton, *Liquids and Liquid Mixtures* (Butterworth, London, 1982).
[13]J. S. Rowlinson and B. Widom, *Molecular Theory of Capillarity* (Claredon Press, 1982).
[14]D. Henderson, *Fundamentals of Inhomogeneous Fluids* (Dekker, New York, 1992).
[15]H. T. Davis, *Statistical Mechanics of Phases, Interfaces, and Thin Films* (VCH, Weinheim, 1996).
[16]D. Frenkel and B. Smit, *Understanding Molecular Simulations*, 2nd ed. (Academic, San Diego, 2002).
[17]J. M. Míguez, M. M. Conde, J.-P. Torré, F. J. Blas, M. M. Piñeiro, and C. Vega, J. Chem. Phys. **142**, 124505 (2015).
[18]W. L. Jorgensen, J. Am. Chem. Soc. **103**, 335 (1981).
[19]W. L. Jorgensen, J. Am. Chem. Soc. **103**, 341 (1981).
[20]W. L. Jorgensen, J. Am. Chem. Soc. **103**, 345 (1981).
[21]J. Chandrasekhar and W. L. Jorgensen, J. Chem. Phys. **77**, 5073 (1982).
[22]J. Chandrasekhar and W. L. Jorgensen, J. Chem. Phys. **77**, 5080 (1982).
[23]W. L. Jorgensen and M. Ibrahim, J. Am. Chem. Soc. **103**, 3976 (1981).
[24]W. L. Jorgensen and J. Tirado-Rives, J. Am. Chem. Soc. **110**, 1657 (1988).
[25]W. L. Jorgensen, D. S. Maxwell, and J. Tirado-Rives, J. Am. Chem. Soc. **118**, 11225 (1996).
[26]J. Helfrich and R. Hentschke, Macromolecules **28**, 3831 (1995).
[27]S. Girard and F. Müller-Plathe, Mol. Phys. **101**, 779 (2003).
[28]S. J. Keasler, S. M. Charan, C. D. Wick, I. G. Economou, and J. I. Siepmann, J. Phys. Chem. B **115**, 11234 (2012).
[29]E. A. Müller and G. Jackson, Annu. Rev. Chem. Biomol. Eng. **5**, 405 (2014).
[30]A. Lymperiadis, C. S. Adjiman, A. Galindo, and G. Jackson, J. Chem. Phys. **127**, 234903 (2007).
[31]A. Lymperiadis, C. S. Adjiman, A. Galindo, and G. Jackson, Fluid Phase Equilib. **274**, 85 (2008).
[32]V. Papaioannou, C. S. Adjiman, G. Jackson, and A. Galindo, Fluid Phase Equilib. **306**, 82 (2011).
[33]G. Mie, Ann. Phys. (Berlin) **316**, 657 (1903).
[34]V. Papaioannou, T. Lafitte, C. Avendaño, C. S. Adjiman, G. Jackson, E. A. Müller, and A. Galindo, J. Chem. Phys. **140**, 054107 (2014).

[35]T. Lafitte, A. Apostolakou, C. Avendaño, A. Galindo, C. S. Adjiman, E. A. Müller, and G. Jackson, J. Chem. Phys. **139**, 154504 (2013).
[36]J. M. Míguez, J. M. Garrido, F. J. Blas, H. Segura, A. Mejía, and M. M. Piñeiro, J. Phys. Chem. C **118**, 24504 (2014).
[37]See https://cdsdt.dl.ac.uk/detherm/ for DECHEMA Gesellschaft für Chemische Technik und Biotechnologie e.V., Frankfurt am Main, Germany (retrieved September, 2015).
[38]E. A. Müller and K. E. Gubbins, Ind. Eng. Chem. Res. **40**, 2193–2211 (2001).
[39]C. McCabe and A. Galindo, "SAFT associating fluids and fluid mixtures," in *Applied Thermodynamics of Fluids*, edited by A. Goodwin, J. V. Sengers, and C. J. Peters (Royal Society of Chemistry, London, 2010), Chap. 8.
[40]C. Avendaño, T. Lafitte, A. Galindo, C. S. Adjiman, G. Jackson, and E. A. Müller, J. Phys. Chem. B **115**, 11154–11169 (2011).
[41]A. Mejía, C. Herdes, and E. A. Müller, Ind. Eng. Chem. Res. **53**, 4131 (2014).
[42]N. S. Ramrattan, C. Avendaño, E. A. Müller, and A. Galindo, Mol. Phys. **113**, 932–947 (2015).
[43]H. Segura, D. Seiltgens, A. Mejía, F. Llovell, and L. F. Vega, Fluid Phase Equilib. **265**, 66 (2008).
[44]H. Segura, D. Seiltgens, A. Mejía, F. Llovell, and L. F. Vega, Fluid Phase Equilib. **265**, 155 (2008).
[45]J. M. Garrido, H. Quinteros-Lama, A. Mejía, J. Wisniak, and H. Segura, Energy **45**, 888–899 (2012).
[46]W. Malesinski, *Azeotropy and Other Theoretical Problems of Vapour-Liquid Equilibrium* (New York Interscience, 1965).
[47]C. Herdes, T. S. Totton, and E. A. Müller, Fluid Phase Equilib. **406**, 91–100 (2015).
[48]C. Herdes, E. E. Santiso, C. James, J. Eastoe, and E. A. Müller, J. Colloid Interface Sci. **445**, 16–23 (2015).
[49]A. Mejía, M. Cartes, H. Segura, and E. A. Müller, J. Chem. Eng. Data **50**, 2928–2941 (2014).
[50]C. Cumicheo, M. Cartes, E. A. Müller, and A. Mejía, Fluid Phase Equilib. **380**, 82–92 (2014).
[51]O. Lobanova, A. Mejía, G. Jackson, and E. A. Müller, J. Chem. Thermodyn. **93**, 320–336 (2016).
[52]R. P. Sear and G. Jackson, Mol. Phys. **81**, 801–811 (1994).
[53]R. P. Sear and G. Jackson, Phys. Rev. E **50**, 386–394 (1994).
[54]E. A. Müller and K. E. Gubbins, Mol. Phys. **80**, 957–976 (1993).
[55]T. Lafitte, C. Avendaño, V. Papaionnou, A. Galindo, C. S. Adjiman, G. Jackson, and E. A. Müller, Mol. Phys. **110**, 1189 (2012).
[56]C. Avendaño, T. Lafitte, C. S. Adjiman, A. Galindo, E. A. Müller, and G. Jackson, J. Phys. Chem. B **117**, 2717–2733 (2013).
[57]O. Lobanova, T. Lafitte, C. Avendaño, E. A. Müller, and G. Jackson, Mol. Phys. **113**, 1228–1249 (2015).
[58]M. P. Allen, *Computer Simulation of Liquids* (Claredon, Oxford, 1987).
[59]D. V. D. Spoel, E. Lindahl, B. Hess, G. Groenhof, A. E. Mark, and H. J. Berendsen, J. Comput. Chem. **26**, 1701 (2005).
[60]G. Galliero, M. M. Piñeiro, B. Mendiboure, C. Miqueu, T. Lafitte, and D. Bessières, J. Chem. Phys. **130**, 104704 (2009).
[61]G. Galliero, J. Chem. Phys. **133**, 074705 (2010).
[62]J. M. Míguez, M. M. Piñeiro, and F. J. Blas, J. Chem. Phys. **138**, 034707 (2013).
[63]M. Dinpajooh, P. Bai, D. A. Allan, and J. I. Siepmann, J. Chem. Phys. **143**, 114113 (2015).
[64]M. A. Cuendet and W. F. van Gunsteren, J. Chem. Phys. **127**, 184102 (2007).
[65]S. Nosé, Mol. Phys. **52**, 255 (1984).
[66]H. J. C. Berendsen, J. P. M. Postma, W. F. van Gunsteren, A. di Nola, and J. R. Haak, J. Chem. Phys. **81**, 3684 (1984).
[67]H. Hulshof, Ann. Phys. (Berlin) **309**, 165 (1901).
[68]E. de Miguel, F. J. Blas, and E. M. del Río, Mol. Phys. **104**, 2919 (2006).
[69]E. de Miguel and G. Jackson, J. Chem. Phys. **125**, 164109 (2006).
[70]H. W. Xiang, *The Corresponding-States Principle and its Practice Thermodynamic. Transport and Surface Properties of Fluids* (Elsevier, Amsterdam, 2005).
[71]B. Widom, J. Chem. Phys. **43**, 3892 (1965).
[72]F. J. Blas, L. G. MacDowell, E. de Miguel, and G. Jackson, J. Chem. Phys. **129**, 144703 (2008).
[73]L. G. MacDowell and F. J. Blas, J. Chem. Phys. **131**, 074705 (2009).
[74]J. G. Sampayo, F. J. Blas, E. de Miguel, E. A. Müller, and G. Jackson, J. Chem. Eng. Data **55**, 4306 (2010).
[75]F. J. Blas, A. I. M.-V. Bravo, J. M. Míguez, M. M. Piñeiro, and L. G. MacDowell, J. Chem. Phys. **137**, 084706 (2012).
[76]C. Vega and E. de Miguel, J. Chem. Phys. **126**, 154707 (2007).
[77]A. D. Cortés-Morales, I. G. Economou, C. J. Peters, and I. J. Siepmann, Mol. Simul. **39**, 1135–1142 (2013).